Time-Dependent Electron Thermal Flux Inhibition in Direct-Drive Laser Implosions

A. Sunahara,[1] J. A. Delettrez,[2] C. Stoeckl,[2] R.W. Short,[2] and S. Skupsky[2]

[1]*Institute of Laser Engineering, Osaka University, 2-6 Yamadaoka, Suita, Osaka 565-0871, Japan*

[2]*Laboratory for Laser Energetics, University of Rochester, 250 East River Road, Rochester, New York 14623-1299, USA*

(Received 11 February 2002; published 28 August 2003)

We simulate direct-drive CH target implosions with square laser pulses by a one-dimensional Fokker-Planck solver combined with a hydrodynamic code, and compare the results with those simulated by the flux-limited Spitzer-Härm model. We find that the electron thermal flux inhibition is time dependent, resulting in longer density scale length, larger laser absorption, and smaller growth of Rayleigh-Taylor instability. The time of peak neutron production calculated from Fokker-Planck simulations agrees with experiments for both 1-ns and 400-ps pulses.

DOI: 10.1103/PhysRevLett.91.095003 PACS numbers: 52.57.Fg, 52.65.–y

Electron thermal conduction plays an important role in inertial confinement fusion (ICF) [1]; it transports the laser energy absorbed near the critical surface into the overdense region and therefore directly affects the ablation, the laser absorption, and implosion dynamics. The flux-limited Spitzer-Härm (SH) model [2] has been widely used to calculate the electron thermal conduction. In this model, the flux limiter f(typical value is 0.06 [3]) is introduced to limit the electron thermal flux given by

$$q_e = \min(f q_{\mathrm{FS}}, q_{\mathrm{SH}}), \tag{1}$$

where q_{FS} is the free-streaming thermal flux defined by $q_{\mathrm{FS}} = n_e T_e (T_e/m_e)^{1/2}$ and q_{SH} is the SH electron thermal flux [4]. The symbols n_e, T_e, and m_e denote, respectively, the electron number density, the electron temperature in energy unit, and the electron mass. Because the flux limiter is empirically determined by comparing the numerical simulation with experimental results, it depends on the experimental conditions and the experimental uncertainties. Many authors have reported that nonlocal electron thermal conduction is important and leads to a flux inhibition in laser-produced plasmas [5–13]. Nonlocal transport models have been developed to include the flux inhibition in hydrodynamic codes [12,13]. For the purpose of carrying out an *ab initio* study of nonlocal thermal conduction and its effect on target implosions, we have developed a Fokker-Planck (FP) code and combined it with the one-dimensional hydrodynamic code LILAC [14]. We show that the flux inhibition is time dependent for square pulses. We also show its effects on the CH target implosion by comparing with the neutron burn history measurements [15].

In our code, the electron velocity distribution function is expanded up to the $\ell = 3$ mode by Legendre polynomials [16] as follows:

Zeroth order:

$$\frac{\partial f_0}{\partial t} + \frac{1}{3}\left\{\frac{v}{\eta x^2}\frac{\partial}{\partial x}(x^2 f_1) - \frac{a_x}{v^2}\frac{\partial}{\partial v}(v^2 f_1)\right\} - \frac{2}{15 v^2}\frac{\partial U}{\partial x}\frac{\partial}{\partial v}(v^3 f_2) = C_{ee} + S_0; \tag{2}$$

First order:

$$\frac{\partial f_1}{\partial t} + v\frac{\partial f_0}{\partial x} - a_x\frac{\partial f_0}{\partial v} + \frac{2}{5}\left\{\frac{v}{x^2}\frac{\partial}{\partial x}(x^2 f_2) - \frac{a_x}{v^3}\frac{\partial}{\partial v}(v^3 f_2)\right\} - \frac{\partial U}{\partial x} f_1 - \left\{\frac{2}{5}\frac{\partial U}{\partial x} + \frac{1}{5x^2}\frac{\partial}{\partial x}(x^2 U)\right\} v^2 \frac{\partial}{\partial v}\left(\frac{f_1}{v}\right) = -\nu_{ei} f_1; \tag{3}$$

Second order:

$$\frac{\partial f_2}{\partial t} + v\frac{\partial f_1}{\partial x} - \frac{v}{3x^2}\frac{\partial}{\partial x}(x^2 f_1) - \frac{2}{3}a_x v\frac{\partial}{\partial v}\left(\frac{f_1}{v}\right) + \frac{3}{7}\left\{v\frac{\partial f_3}{\partial x} - \frac{a_x}{v^4}\frac{\partial}{\partial v}(v^4 f_3)\right\} + \frac{1}{7}\left\{\frac{2}{x^2}\frac{\partial(x^2 U)}{\partial x} - 4\frac{\partial U}{\partial x}\right\} f_2 - \left\{\frac{\partial U}{\partial x} - \frac{1}{3x^2}\frac{\partial(x^2 U)}{\partial x}\right\} v\frac{\partial f_0}{\partial x} - \frac{1}{21}\left\{8\frac{\partial U}{\partial x} + \frac{3}{x^2}\frac{\partial(x^2 U)}{\partial x}\right\} v\frac{\partial f_2}{\partial v} = -3\nu_{ei} f_2; \tag{4}$$

Third order:

$$\frac{\partial f_3}{\partial t} + \frac{3}{5}\left\{v\frac{\partial f_2}{\partial x} - a_x v^2\frac{\partial}{\partial v}\left(\frac{f_2}{v^2}\right)\right\} = -6\nu_{ei} f_3; \tag{5}$$

where f_0, f_1, f_2, and f_3 are the $\ell = 0$, 1, 2, and 3 mode of the distribution function, respectively. For the closure of these coupled equations, we use the simplified f_3 equation without the correction terms for the hydrodynamic motion and spherical geometry; f_3 is reset to zero at the beginning of every time step. C_{ee} is the electron-electron collision operator [17] determined by the self-interaction

of f_0; ν_{ei} is the electron-ion collision frequency [11] given by $\nu_{ei} = \phi 4\pi n_e Z^* e^4 \ln\Lambda / m_e^2 v^3$, which effectively includes corrections of higher-order terms neglected in C_{ee}, and $\phi = (Z^* + 4.2)/(Z^* + 0.24)$. The effective charge Z^* is defined by $Z^* = \langle Z^2 \rangle / \langle Z \rangle$, where Z is the charges of ion species and $\langle\ \rangle$ indicates averaging over the ion species. The symbols e, $\ln\Lambda$, and U are the electron charge, Coulomb logarithm [18], and ion velocity, respectively. The acceleration term is defined as $a_x = eE_x/m_e$, where the electric field E_x is obtained from the current free condition $j = (4\pi e/3) \int_0^\infty dv v^3 f_1 = 0$. S_0 is a source term that accounts for changes caused by the electron density and temperature from ionization, radiation transport, laser absorption, and the work done by pressure. These are calculated by the LILAC code prior to FP calculations. S_0 depends on f_0, but we approximated it by $S_0 \Delta t = \delta(f_M)$, where f_M is the Maxwell distribution function. Here, for the laser absorption in S_0, we applied Langdon's reduction factor [19] to both FP and SH, although we did not apply the exact Langdon operator to f_0 in Eq. (2). We caution that this would possibly further decrease the heat flux [20]. The dimensionless factor η corrects the ideal gas heat capacity used in the FP equation to be consistent with the real heat capacity C_{ve} obtained from the hydrodynamic code. Taking the v^2 moment in Eq. (2) using only the configuration-directional term leads to the equation of the thermal conduction with $C_{ve} = (3/2)\eta n_e$, to be $C_{ve} dT_e/dt = \mathrm{div} q_e$. After the FP calculation, the effective electron temperature, T_{eff} defined as $T_{\mathrm{eff}} = (4\pi m_e/3n_e) \int_0^\infty v^4 f_0 dv$, is returned to LILAC.

We simulated an implosion of a polystyrene CH shell of 900-μm diameter and 20-μm thickness filled with 15 atm of D_2 gas. The 0.35-μm-wavelength laser pulse is a 1-ns-duration square with a rise time (0 to maximum) of 400 ps and a constant power of 25 TW between 0.4 to 1.4 ns. The irradiation intensity on the target is 9×10^{14} W/cm^2. Figure 1(a) shows the laser profile, together with the calculated electron thermal flux at the critical surface, $q_{\mathrm{FP}} = (2\pi m_e/3) \int_0^\infty v^5 f_1 dv$, normalized by the free-streaming thermal flux at the critical surface, q_{FS}. The ratio $q_{\mathrm{FP}}/q_{\mathrm{FS}}$ can be defined as the flux-inhibition factor f, if we assume q_{FP} to be the "actual" flux q_e, when $f q_{\mathrm{FS}} \leq q_{\mathrm{SH}}$ in Eq. (1). We observe that f increases until 400 ps and then decreases with time. To explain this time dependence of f using the properties of the SH model, we consider the time dependence of the relation between q_{FS} and q_{SH}, described by the SH model. q_{SH} is written in terms of λ_0/L_T and the free-streaming flux as $q_{\mathrm{SH}} = 16\sqrt{2}\pi^{-1/2}(\lambda_0/L_T) q_{\mathrm{FS}}$. Here λ_0 is the electron mean free path for 90° collision scattering given by $\lambda_0 = v_{\mathrm{th}}^4/[4\phi\pi n_e Z^* (e^2/m_e)^2 \ln\Lambda]$, where $v_{\mathrm{th}} = (2T_e/m_e)^{1/2}$. L_T is the temperature gradient scale defined as $T_e/(\partial T_e/\partial x)$. Figure 1(b) shows the temporal evolution of λ_0/L_T, q_{FS}, q_{SH}, and q_{FP} at the critical surface. λ_0/L_T increases during the rise time of the laser pulse when T_e increases rapidly, and then decreases since L_T increases faster than λ_0 after 400 ps, when the constant laser pulse begins. On the other hand, q_{FS} keeps increasing beyond 400 ps as T_e increases. Consequently, q_{SH}, a function of the product of λ_0/L_T and q_{FS}, stays almost constant after 400 ps. As seen in Fig. 1(b), the trends of q_{SH} and q_{FP} are similar, and the ratio $q_{\mathrm{FP}}/q_{\mathrm{SH}}$ stays between 0.5 and 0.6 in the range of the constant laser power in spite of the decrease of λ_0/L_T. This indicates that nonlocality of the electron transport increases with time and overcomes the decrease of λ_0/L_T, thus keeping the ratio $q_{\mathrm{FP}}/q_{\mathrm{SH}}$ constant. From the time development of f in Fig. 1(a) and the absorbed laser power I_A, we estimate the absorbed laser power-averaged flux-inhibition factor $\langle f \rangle = \int f I_A dt / \int I_A dt$ to be 0.075 for the sharp-cutoff, flux-limited SH formula of Eq. (1). We also calculated $\langle f \rangle$ with the harmonic mean flux-limited SH model, which is given by $q_e^{-1} = (f q_{\mathrm{FS}})^{-1} + q_{\mathrm{SH}}^{-1}$, and obtained $\langle f \rangle = 0.15$.

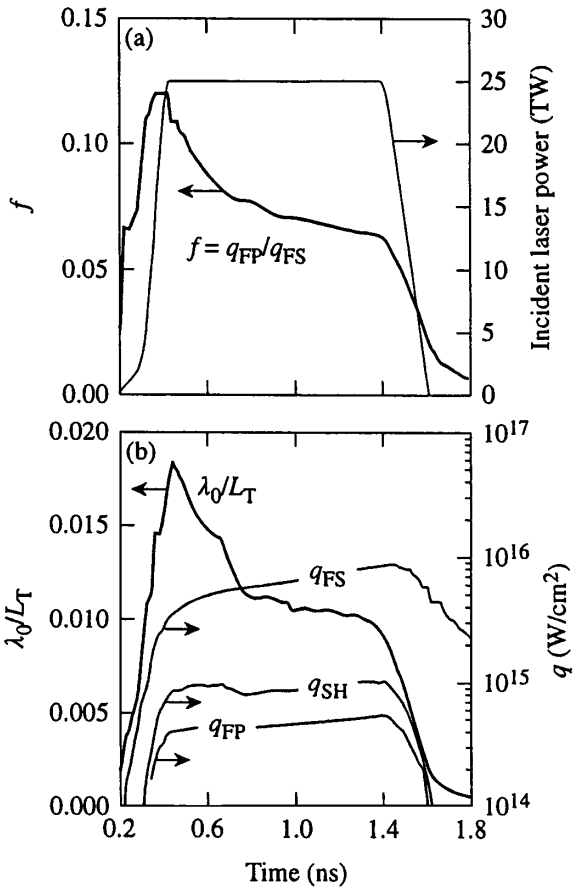

FIG. 1. (a) Ratio of q_{FP} to q_{FS} calculated at the critical surface, together with the laser profile, and (b) ratio of λ_0 to L_T. q_{SH} and q_{FS} are calculated from n_e and T_e obtained from FP calculations.

We checked the validity of our FP calculations by comparing the calculated neutron burn history with experimental results. We also compared the burn history with the results of the constant flux-limited SH model.

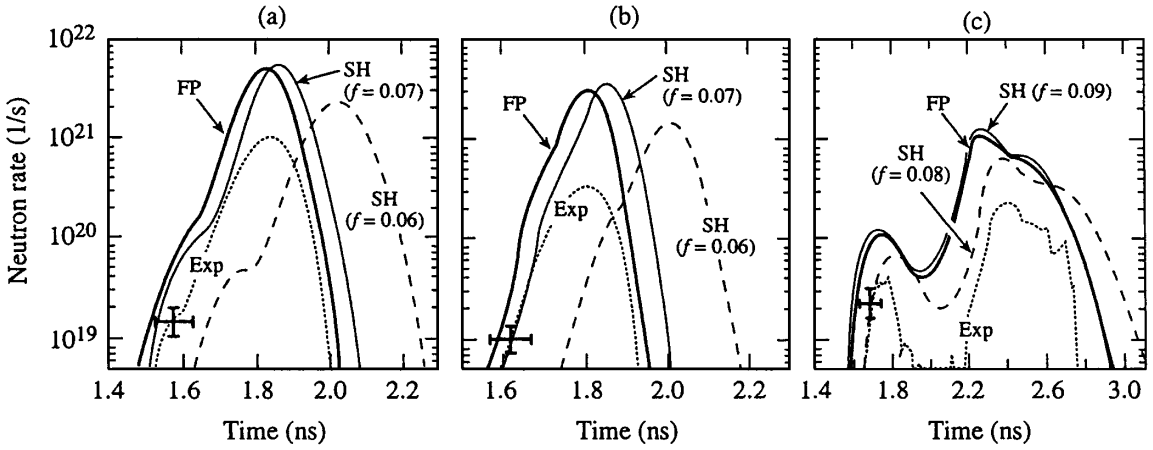

FIG. 2. Comparison of neutron rates calculated by FP and SH of $f = 0.07$ and 0.06. (a) 15 atm of D_2 fuel gas and 1-ns square pulse, (b) 3 atm of D_2 fuel gas and 1-ns square pulse, and (c) 20 atm of DT fuel and 0.4-ns square pulse.

The experiments were performed on the 60-beam OMEGA laser system [21] with the best smoothing conditions [22]. The neutron burn history was measured with the neutron temporal detector, which has a temporal accuracy of ± 50 ps [15]. All of the calculations were carried out with the real laser pulse and target condition. Figures 2(a)–2(c) show three neutron rates calculated by FP and by the flux-limited SH model. The gas pressure was 15 atm of D_2 in Fig. 2(a), 3 atm of D_2 in Fig. 2(b), and 20 atm of DT in Fig. 2(c). The shell thickness was 20 μm. The shell was irradiated by a square pulse, whose duration time was 1 ns in Figs. 1(a) and 1(b) and 0.4 ns in Fig. 2(c). The results of FP and SH with $f = 0.07$ in Figs. 2(a) and 2(b) show good agreement with the experimental results, better than for the typical value of $f = 0.06$. The reduced measured burn history is believed to be caused by the shell-fuel mix during the deceleration phase due to the Rayleigh-Taylor (RT) instability [23]. The results in Figs. 2(a) and 2(b) are consistent with those shown in Fig. 1(a), where the FP calculation gives $\langle f \rangle = 0.075$. For the case of a 400-ps square-pulse in Fig. 2(c), the experimental neutron burn history lies between the FP result and the SH with $f = 0.08$. In this case, $\langle f \rangle$ was found to be 0.087, which is larger than 0.075 for the 1-ns duration pulse in Figs. 2(a) and 2(b), indicating that a larger flux-inhibition factor is needed when the pulse duration is shorter. This is also consistent with the fact that a larger flux-inhibition factor is needed to match the flux-limited SH flux to FP early in the pulse, as shown in Fig. 1(a). In all of the cases shown in Figs. 2(a)–2(c), FP gives neutron temporal profiles about 50 ps ahead of these experiments, which is within the experimental error bar. We surmise that a stricter treatment of S_0 and η in Eq. (2) might reduce this discrepancy.

Next, we show effects of the time dependence of f on the absorption and the stability of the shell during the 1-ns square-pulse implosion. The fact that FP gives a larger thermal flux than SH with $f = 0.07$, as shown in Fig. 1(a), results in a larger electron density scale length $L_n = n_e/(\partial n_e/\partial x)$ at the critical surface as seen in Fig. 3. The larger L_n produces a larger absorption fraction by inverse bremsstrahlung, whereas T_e calculated by FP and SH with $f = 0.07$ in Fig. 3 are close. In Fig. 4 we show the temporal evolution of the laser absorption calculated by FP and by SH with $f = 0.07$ and 0.06. The laser power absorption calculated by FP is larger early in the pulse, while later in the pulse, FP gives a lower laser absorption than SH with $f = 0.07$. The total absorption fraction is 0.83 for FP and 0.76 and 0.68 for SH with f of 0.07 and 0.06, respectively. FP gives a larger laser absorption fraction than that of the SH with $f = 0.07$ and 0.06 by about 7% and 15%, respectively.

The effect of the FP transport on the growth of the RT instability in the acceleration phase was investigated using the Betti-Goncharov formula [23]. The averaged ablation density $\langle \rho_a \rangle$ and the averaged mass ablation rate $\langle \dot{m} \rangle$ are 3.3 g/cm^3 and 1.35×10^6 g/cm^{2}s for FP and

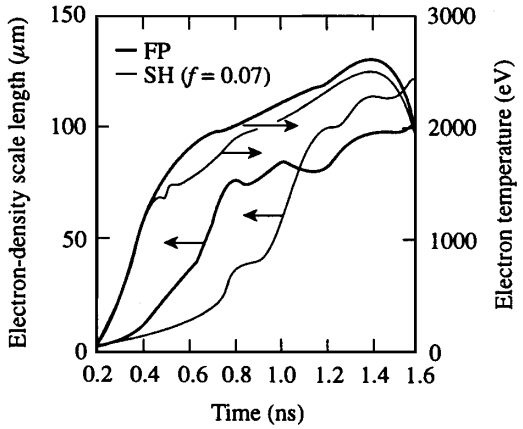

FIG. 3. Electron-density scale length L_n and thermal electron temperature T_e at the critical surface, calculated by FP and SH of $f = 0.07$.

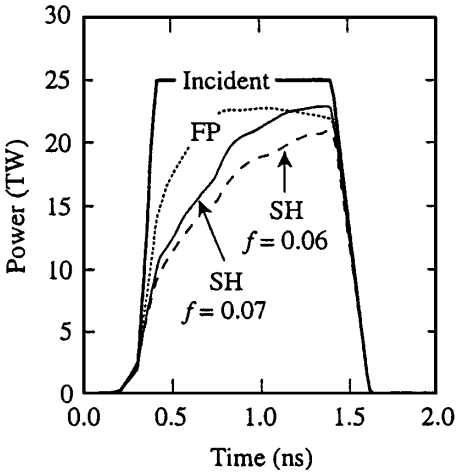

FIG. 4. Absorbed laser power calculated by FP and SH of $f = 0.07$ and 0.06. As a reference, the incidental power is also shown.

3.9 g/cm^3 and 1.53×10^6 g/cm^{2}s for SH with $f = 0.07$. Here, FP gives $\langle \rho_a \rangle$ and $\langle \dot{m} \rangle$ about 15% lower than that for SH. The averaged minimum density-gradient scale length $\langle L_m \rangle$ is 1.47 μm for FP and 1.06 μm for SH. The fast electrons resulting from nonlocal heat flow contributes partly to the increase of $\langle L_m \rangle$. However, the increase of isentrope by shock wave and radiation [24] is more effective in the current condition for the CH target. The difference of the temporal dependence of the electron heat flux between FP and SH leads to different time evolution of the density scale length at the ablation front, resulting in a larger value in FP calculation. The larger $\langle L_m \rangle$ in FP leads to stabilization of the growth of the Rayleigh-Taylor instability of short-wavelength perturbations during the acceleration phase. The obtained α and β in the Betti-Goncharov formula [23] are 0.90 and 1.5, which are almost the same for both FP and SH. The resultant e foldings of the RT growth are 6.1 for FP and 7.5 for SH. This lowering of RT growth due to nonlocal transport was also confirmed by the experiments [25] for the 0.53-μm-wavelength laser.

In conclusion, we found that the flux inhibition for the square-pulse CH implosion is time dependent. The FP calculation yielded the thermal flux at the critical surface early in the pulse larger than that in the flux-limited SH with a constant flux limiter equivalent to the average value calculated from the FP calculation. Neutron burn histories calculated by FP agree well for experiments with different laser pulse durations, indicating the need for a larger fiux limiter in SH calculation at the short pulse duration. The increase in the density scale length at the critical surface shown by FP calculation increases laser absorption. The increased scale length at the ablation region tends to slightly stabilize the Rayleigh-Taylor growth for short-wavelength perturbations.

This work was supported by the U.S. Department of Energy, Office of Inertial Confinement Fusion, under Cooperative Agreement No. DE-FC03-92SF19460, New York State Energy Research and Development Authority, and the Japan Society for Promotion of Science.

[1] J. Nuckolls *et al.*, Nature (London) **239**, 139 (1972).
[2] R. C. Malone, R. L. McCrory, and R. L. Morse, Phys. Rev. Lett. **34**, 721 (1975).
[3] R. L. McCrory *et al.*, in *High Intensity Laser-Matter Interactions*, edited by E. M. Campbell and H. Baldis (SPIE, Bellingham, WA, 1988), Vol. 913, p. 40.
[4] L. Spitzer, Jr. and R. Härm, Phys. Rev. **89**, 977 (1953).
[5] R. J. Mason, Phys. Rev. Lett. **47**, 652 (1981).
[6] A. R. Bell, R. G. Evans, and D. J. Nicholas, Phys. Rev. Lett. **46**, 243 (1981).
[7] J. P. Matte and J. Virmont, Phys. Rev. Lett. **49**, 1936 (1982).
[8] J. R. Albritton, Phys. Rev. Lett. **50**, 2078 (1983).
[9] J. P. Matte *et al.*, Phys. Rev. Lett. **53**, 1461 (1984).
[10] A. Nishiguchi *et al.*, Phys. Fluids B **4**, 417 (1992).
[11] E. M. Epperlein, Laser Part. Beams **12**, 257 (1994).
[12] J. F. Luciani, P. Mora, and J. Virmont, Phys. Rev. Lett. **51**, 1664 (1983).
[13] E. M. Epperlein and R. W. Short, Phys. Fluids B **3**, 3092 (1991).
[14] M. C. Richardson *et al.*, in *Laser Interaction and Related Plasma Phenomena*, edited by H. Hora and G. H. Miley (Plenum Publishing, New York, 1986), Vol. 7, p. 421.
[15] R. A. Lerche, D. W. Phillion, and G. L. Tietbohl, Rev. Sci. Instrum. **66**, 933 (1995).
[16] I. P. Shkarofsky, T. W. Johnston, and M. P. Bachynski, *The Particles Kinetics of The Plasmas* (Addison-Wesley, Reading, Massachusetts, 1966).
[17] E. M. Epperlein, J. Comput. Phys. **112**, 291 (1994).
[18] S. Skupsky, Phys. Rev. A **36**, 5701 (1987).
[19] A. B. Langdon, Phys. Rev. Lett. **44**, 575 (1980).
[20] P. Mora and H. Yahi, Phys. Rev. A **26**, 2259 (1982).
[21] T. R. Boehly *et al.*, Opt. Commun. **133**, 495 (1997).
[22] D. D. Meyerhofer *et al.*, Phys. Plasmas **8**, 2251 (2001).
[23] R. Betti *et al.*, Phys. Plasmas **5**, 1446 (1998).
[24] R. Betti *et al.*, Phys. Plasmas **3**, 2122 (1996).
[25] T. Sakaiya *et al.*, Phys. Rev. Lett. **88**, 145003 (2002).